

Heterogeneous & Homogeneous & Bio- & Nano-

CHEM **CAT** CHEM

CATALYSIS

Accepted Article

Title: Electrospun BiOCl/Bi₂Ti₂O₇ nanorod heterostructures with enhanced solar light efficiency in photocatalytic degradation of tetracycline hydrochloride

Authors: Yuxian Xu, Daifeng Lin, Xinping Liu, Yongjin Luo, Hun Xue, Baoquan Huang, Qinghua Chen, and Qingrong Qian

This manuscript has been accepted after peer review and appears as an Accepted Article online prior to editing, proofing, and formal publication of the final Version of Record (VoR). This work is currently citable by using the Digital Object Identifier (DOI) given below. The VoR will be published online in Early View as soon as possible and may be different to this Accepted Article as a result of editing. Readers should obtain the VoR from the journal website shown below when it is published to ensure accuracy of information. The authors are responsible for the content of this Accepted Article.

To be cited as: *ChemCatChem* 10.1002/cctc.201800100

Link to VoR: <http://dx.doi.org/10.1002/cctc.201800100>

Electrospun BiOCl/Bi₂Ti₂O₇ nanorod heterostructures with enhanced solar light efficiency in photocatalytic degradation of tetracycline hydrochloride

Yuxian Xu,^[a] Daifeng Lin,^[a] Xinping Liu,^[a] Yongjin Luo*,^[a] Hun Xue,^[a] Baoquan Huang,^[a]

Qinghua Chen,^[a,b] and Qingrong Qian*^[a]

Abstract: Bismuth titanates (BTs) can be fabricated via electrospinning combined with calcination at different temperatures. BiOCl/Bi₂Ti₂O₇ nanorod heterostructures were obtained at 500 °C. It possesses excellent photocatalytic efficiency and stability for tetracycline hydrochloride (TC-HCl) degradation under simulated solar light. The excellent catalytic activity is predominantly attributed to the heterostructure between BiOCl and Bi₂Ti₂O₇, which accelerates the separation of photogenerated carriers while narrow band gap of Bi₂Ti₂O₇ enhances solar energy utilization. On the basis of energy band engineering, scavenger tests and LC-HRMS analysis, the possible degradation pathway of TC-HCl and photocatalytic mechanism were proposed. Our work can predict a facile route for achieving high photocatalytic performance of Bi₂Ti₂O₇ based materials in the application of TC-HCl degradation.

Introduction

Recently, antibiotic has been widely used as antibacterial agents in human and veterinary medicine for treatment of bacterial infection.^[1] A survey research had indicated that total production of all antibiotics in China was estimated to be 248000 tons, the total usage for the 36 chemicals was 92700 tons, and estimated 53800 tons of them entered into the receiving environment (46% received by water) following various wastewater treatments in 2013.^[2] Amongst the different antibiotics, tetracycline antibiotics (TCs) are ranked second in the production and usage of antibiotics worldwide and are ranked first in China due to their low cost, ease of use and relatively minor side effects.^[3] However, tetracycline antibiotics residues in the environment have adverse effects on organisms, contamination of food and drinking water, and increased bacterial resistance.^[4] Unfortunately, most of the wastewater treatment plants are not capable to remove TCs effectively.^[5] Therefore, it is imperative to develop alternative processes to remove TCs from waters.

Semiconductor photocatalysis offers great potential opportunities to remove TCs from waters due to its high efficiency, no secondary pollution and low cost. However, there are still some problems, the major drawback of which is that

most of the semiconductor photocatalysts possess wide band gaps and could only work under UV light irradiation (~4% of solar energy).^[6] Accordingly, it is necessary to search new and efficient visible-light-driven photocatalysts for TCs degradation. Recently, Bi-based semiconductors, such as BiOX (X = Br, I)^[7], Bi_xO_yX_z (X = Cl, I)^[8], Bi₂MO₆ (M = W, Mo)^[9], Bi₂O₂CO₃^[10] and bismuth titanate, as new promising visible light photocatalysis candidates are particularly interesting. Among bismuth titanate, Bi₂Ti₂O₇, with a narrow band gap of 2.90 eV^[11] and good chemical stability^[12], is a very suitable candidate of semiconductor for visible light photocatalysis. However, the photocatalytic capability of Bi₂Ti₂O₇ is not efficient enough to meet the application requirement due to the low separation efficiency of the photoexcited electron-hole pairs. To address this issue, building heterojunction with a suitable semiconductor is an effective strategy.^[13] To date, Bi₂Ti₂O₇ based heterojunction photocatalysts, such as Bi₂Ti₂O₇/TiO₂^[14] and Bi₂Ti₂O₇/Bi₄Ti₃O₁₂^[15], have been studied to enhance the photocatalytic efficiency for degradation of dye pollutants in water treatment. Amongst the various Bi-based semiconductors, BiOCl have attracted tremendous attention owing to its layered structure. The {Cl-Bi-O-Bi-Cl} sheets structure benefits the photogenerated electron-hole pairs separation and transport process although it has a wide band gap.^[16] Considering that the valence band maximum (VBM) and conduction band minimum (CBM) potentials of BiOCl are both more positive than those of Bi₂Ti₂O₇, the construction of BiOCl/Bi₂Ti₂O₇ heterostructure is feasible. Lately, K. V. Pham et.al prepared BiOCl/Bi₂Ti₂O₇ by hydrothermal method in combination with an annealing process, and found BiOCl/Bi₂Ti₂O₇ nanocomposite shows higher photocatalytic activity than pure BiOCl and Bi₂Ti₂O₇.^[17] But that BiOCl can be excited by visible light in above work is controversial to the wide band gap of BiOCl^[12].

On the other hand, it has been reported that 1D nanostructures, such as nanowires, nanotubes and nanorods, are beneficial for charge transport.^[18] To bring out the superiority of the nanostructures, constructing 1D BiOCl/Bi₂Ti₂O₇ nanostructures is meaningful. Electrospinning as a remarkably simple and versatile technique for preparing well-defined 1D nanostructured materials, has been widely used to fabricate many catalysts.^[19] Previously, we have successfully synthesized a series of 1D nanostructured oxide by electrospinning technology, including LaOCl, TiO₂ and LaCoO₃.^[20]

In this work, we fabricated PVP/BiCl₃/Ti(OiPr)₄ composite nanofibers via electrospinning first, and bismuth titanates (BTs) with different phase can be obtained by tuning calcination temperature. For example, calcination at 400 or 500 °C can obtain heterostructured BiOCl/Bi₂Ti₂O₇, while 600 or 700 °C gives rise to Bi₂Ti₄O₁₁/Bi₂Ti₂O₇. The results of tetracycline hydrochloride (TC-HCl) photodegradation show that a 500 °C calcination of PVP/BiCl₃/Ti(OiPr)₄ composite nanofibers exhibit the best photocatalytic activity, approximate 90% of TC-HCl can

[a] Y. Xu, D. Lin, Prof. Dr. X. Liu, Prof. Dr. Y. Luo, Prof. Dr. H. Xue, Prof. Dr. B. Huang, Prof. Dr. Q. Chen, Prof. Dr. Q. Qian
Environment Science and Engineering, Fujian Normal University,
Fujian

Key Laboratory of Pollution Control & Resource Reuse, Fuzhou
350007,
China

[b] Prof. Dr. Q. Chen
Fuqing Branch of Fujian Normal University, Fuqing, Fujian 350300,
China

E-mail: yongjinluo@fjnu.edu.cn (Y. Luo), qrqian@fjnu.edu.cn (Q. Qian)
Supporting information for this article is given via a link at the end of the document.

FULL PAPER

WILEY-VCH

be removed within 2 h. Moreover, the possible degradation pathway of TC-HCl and photocatalytic mechanism were study in detail.

Results and Discussion

The morphology of BTs is observed through SEM images. Fig.1a shows the PVP/BiCl₃/Ti(OiPr)₄ composite nanofibers are continuous and smooth with a diameter of approximate 20-100 nm. After calcination at 300 °C, the composite nanofibers are still smooth, but accompanied with some breakage and bend of nanofibers (Fig.1b). As the temperature rises to 400 °C (Fig.1c), most nanofibers have been broken into nanorods. Further increasing temperatures to 500-700 °C (Fig.1d-f), no obvious change is observed expect that nanorods become thicker. The textural properties (specific surface areas, pore volume and average pore diameter) of BTs are summarized in Table 1. With raising the calcination temperature from 300 °C to 700 °C, the specific surface areas increase first and then decreases. BT-500 exhibits an apparent the largest surface area. The higher surface area of BT-500 will probably adsorb more irradiation photons and target pollutant and thus favors the photocatalytic activity.^[21]

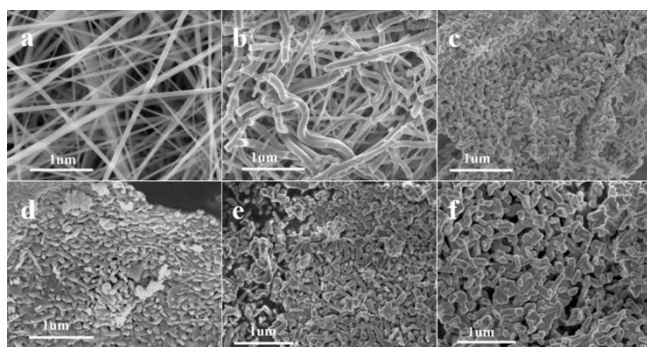


Figure 1. SEM images of (a) PVP/BiCl₃/Ti(OiPr)₄ composite nanofibers; (b) BT-300, (c) BT-400, (d) BT-500, (e) BT-600, (f) BT-700.

Table 1. Textural properties and the values of O_{II}/O_I of samples

Sample	S _{BET} (m ² /g) ^a	Pore volume (cm ³ /g) ^a	Average pore diameter (nm) ^a	O _{II} /O _I ^b	K(h ⁻¹) ^c
BT-300	4	0.015	4.4		0.05
BT-400	20	0.142	3.9	0.21	0.75
BT-500	21	0.120	12.5	0.29	0.95
BT-600	9	0.089	16.3	0.18	0.55
BT-700	5	0.023	3.9	0.14	0.41

^a Deduced from N₂ adsorption-desorption curves.

^b Deduced from XPS analysis.

^c Deduced from the pseudo-first equation.

The phase analysis of BTs is performed using XRD and is reported in Fig.2. It is clearly that various diffraction peaks are observed in different BTs. The diffraction peaks of BT-300 at 12.0°, 25.9°, 32.5°, 33.5°, 46.7° and 49.7°, are corresponding to

the respective (001), (101), (110), (102), (200) and (113) planes of BiOCl (JCPDS no. 85-0861, marked with “♦”). Additional peaks (14.8°, 28.7°, 34.7°, 38.0° and 49.9°) attributed to Bi₂Ti₂O₇ (JCPDS no. 32-0118, marked with “▲”) can be found for BT-400. With increasing temperature to 500 °C, the XRD peaks intensity of Bi₂Ti₂O₇ become stronger as the amount of Bi₂Ti₂O₇ increases. Further raising the calcination temperature to 600 °C or 700 °C, the diffraction peaks of Bi₂Ti₂O₇ is retained, but BiOCl phase has been replaced with Bi₂Ti₄O₁₁ phase (JCPDS no. 15-0325, marked with “●”). The results may cause by BiOCl gradually decomposes to form Bi₂O₃ and BiCl₃ gas with the increase of temperature.^[22]

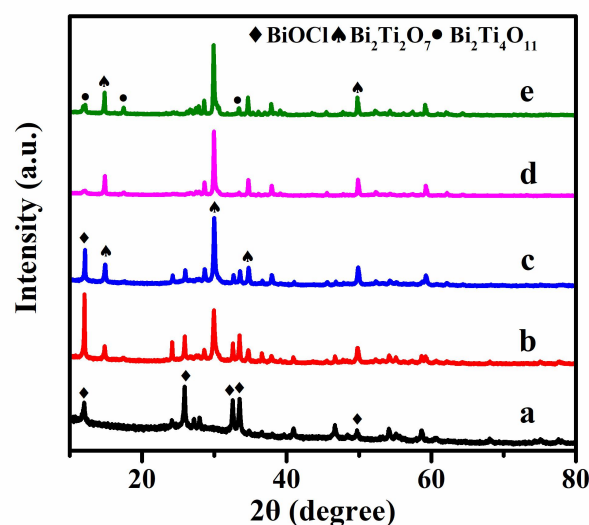


Figure 2. XRD patterns of BTs: (a) BT-300, (b) BT-400, (c) BT-500, (d) BT-600, (e) BT-700.

More detailed information regarding the chemical environment of Bi, Ti and O in samples is ascertained using XPS. As observed in Fig. 3A, the binding energies at positions around 159.3 and 164.6 eV can be attributed to Bi 4f_{7/2} and Bi 4f_{5/2}, respectively. The two peaks with a typical Bi 4f spin-orbit splitting of 5.3 eV is characteristic of Bi³⁺.^[23] With the increase in the calcination temperature, these peaks of Bi 4f clearly shift toward the low band energy, which plausibly caused by Bi-O-Cl system transits to Bi-O-Ti system. As for Ti 2p element (Fig. 3B), two peaks at 458.2 and 464.6 eV for BT-300 are assigned to Ti 2p_{1/2} and Ti 2p_{3/2}, respectively, which is corresponding to Ti⁴⁺ in pure TiO₂.^[24] Combine with XRD analysis, BT-300 consists of BiOCl and unreacted TiO₂, which illustrates that Bi-O-Ti system cannot be fabricated at low calcination temperature. For other samples, the binding energy of Ti 2p has a slight shift toward the high band energy, due to the decreasing electron density around the Ti⁴⁺ in the forming Bi-O-Ti bands.^[25] From the XRD and XPS analysis, we can deduce that the phase transformation to BiOCl/Bi₂Ti₂O₇ form BiOCl/TiO₂, and then transfers to Bi₂Ti₄O₁₁/Bi₂Ti₂O₇.

The O 1s spectrum region shows two peaks with approximately binding energies of 531 eV and 530.0 eV (Fig. 3C). Because the weight contents of C in BT-300 is 39.65%, the peaks of BT-300 should correspond to C=O bond^[26] and the lattice O of samples, respectively. However, increasing the calcination temperature to 400-700 °C, the two peaks should

FULL PAPER

WILEY-VCH

belong to surface-adsorbed hydroxyl groups (O_{II}) and the lattice O (O_I). It has been generally accepted that O_{II} species play an important role in photocatalytic degradation. As seen in table 1, BT-500 shows the largest molar ratio of O_{II}/O_I than other samples, indicating the more hydroxyl groups in BT-500 can react with photogenerated holes and facilitate separation of photogenerated charges.

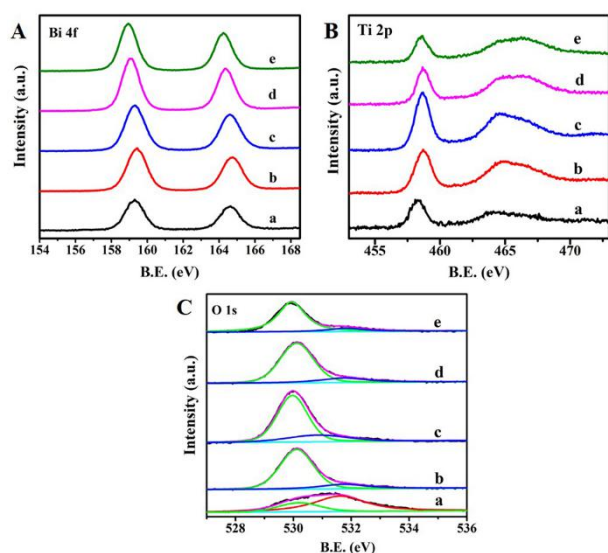


Figure 3. High-resolution XPS spectra of (A) Bi, (B) Ti, and (C) O for BTs: (a) BT-300, (b) BT-400, (c) BT-500, (d) BT-600, (e) BT-700.

Photocatalytic performance is evaluated for degradation of TC-HCl aqueous solution under simulated solar irradiation. As seen in Fig. 4A, the degradation efficiency of TC-HCl without catalyst is approximately 6% after 2 h, suggesting that the TC-HCl degradation is indeed induced by photocatalysis.^[27] BT-300 shows poor photodegradation efficiency (~10%) after illumination for 2 h. This may result from too much carbonaceous residue in BT-300, occupying active sites and reducing the utilization of the light.^[28] In contrast, under the same illumination time, the removal rates can be reached as high as 81% and 90% over BT-400 and BT-500, respectively. However, the removal rate reduces to 68% for BT-600 and 57% for BT-700. In addition, the pseudo-first-order model^[29] is applied to quantitatively compare the reaction kinetics of decomposition rate of TC-HCl. The various rate constant (k) is depicted in the form of columns of different colors (Fig. 4B) and shows in table 1. It can be seen from the diagram that the catalytic efficiency of BT-500 is 19.0 and 1.75 times higher than that of BT-300 and BT-600, respectively. Therefore, $\text{BiOCl}/\text{Bi}_2\text{Ti}_2\text{O}_7$ has better photocatalytic activity than $\text{Bi}_2\text{Ti}_4\text{O}_{11}/\text{Bi}_2\text{Ti}_2\text{O}_7$, and more $\text{Bi}_2\text{Ti}_2\text{O}_7$ content in $\text{BiOCl}/\text{Bi}_2\text{Ti}_2\text{O}_7$ enhances the photocatalytic performance. Moreover, as seen Table S1, the observed photocatalytic performance of BT-500 is better than most of the reported $\text{Bi}_2\text{Ti}_2\text{O}_7$ based semiconductors.

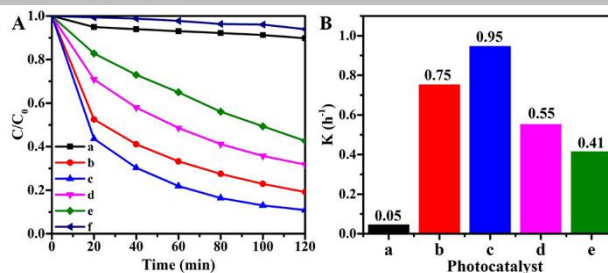


Figure 4. (A) Degradation curves of TC-HCl, (B) apparent rate constants for degradation of TC-HCl under solar light irradiation over BTs: (a) BT-300, (b) BT-400, (c) BT-500, (d) BT-600, (e) BT-700, (f) Blank.

UV/vis diffuse reflectance spectra are measured to characterize the optical bandgap and absorption capability of the as-prepared photocatalysts. As seen in Fig. 5, BT-300 absorbs light of all wavelengths, which could be due to the high C contents and the color of sample is black. BT-400, BT-500, BT-600 and BT-700 all exhibit an obvious spectra absorption in the visible light region. The band gap energy can be obtained from the plots of $(A\text{h}\nu)^{1/2}$ versus $h\nu$ (in the inset of Fig. 5). The band gap values for BT-400, BT-500, BT-600 and BT-700 are 2.58, 2.54, 2.68 and 2.78 eV, respectively. Meanwhile, the intensity of absorption for BT-400 and BT-500 are higher than that for BT-600 and BT-700 in 200-800 nm, which can be expected to the better utilization of solar light for photocatalytic reaction.^[30]

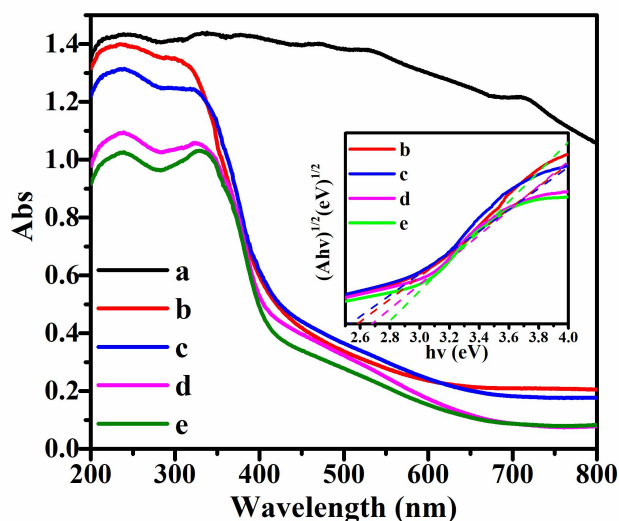


Figure 5. UV-vis diffuse reflectance spectra of BTs: (a) BT-300, (b) BT-400, (c) BT-500, (d) BT-600, (e) BT-700. The inset is band-gap evaluation from the plot of $(A\text{h}\nu)^{1/2}$ versus $h\nu$.

The rapid recombination of photogenerated electron-hole pairs is main drawback of $\text{Bi}_2\text{Ti}_2\text{O}_7$. PL spectra are performed to observe the separation rate of the photogenerated electron-hole pairs. The lower PL intensity often reflect the higher separation efficiency of the charge carriers.^[31] The PL intensity of BTs is in the order of BT-300 > BT-700 > BT-600 > BT-400 > BT-500 (Fig. 6A). To provide additional evidence, the transient photocurrent responses of BTs electrodes are recorded for several on-off cycles, and the results are shown in Fig. 6B. All samples exhibit fast and reproducible transient photocurrent responses under

FULL PAPER

WILEY-VCH

several on-off cycles of intermittent simulated solar irradiation. The photocurrent density of BT-300, BT-400, BT-500, BT-600 and BT-700 are about 0.049-0.040, 1.00-0.65, 1.15-0.66, 0.074-0.066, 0.068-0.050 $\mu\text{A cm}^{-2}$, respectively. It is notable that BT-400 and BT-500 have a better reproducible photocurrent response. Therefore, $\text{BiOCl}/\text{Bi}_2\text{Ti}_2\text{O}_7$ has higher separation efficiency of the charge carriers than $\text{Bi}_2\text{Ti}_4\text{O}_{11}/\text{Bi}_2\text{Ti}_2\text{O}_7$. Amongst BTs, BT-500 has the lowest PL intensity and the highest photocurrent density. That is, BT-500 has the highest separation efficiency of photogenerated electron-hole pairs and greatly facilitate its photocatalytic activity.

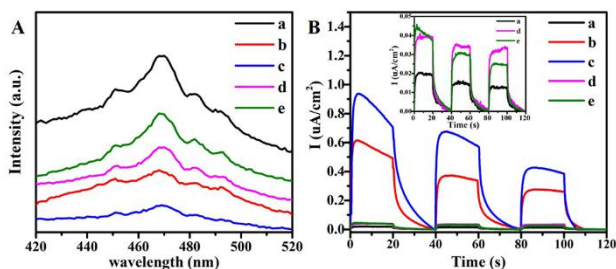


Figure 6. (A) PL spectra and (B) Transient photocurrent response for BTs: (a) BT-300, (b) BT-400, (c) BT-500, (d) BT-600, (e) BT-700.

Compared with $\text{Bi}_2\text{Ti}_2\text{O}_7/\text{Bi}_2\text{Ti}_4\text{O}_{11}$, $\text{BiOCl}/\text{Bi}_2\text{Ti}_2\text{O}_7$ could effectively inhibit the electron-hole pair recombination which may cause energy band engineering. According to the references,^[12, 32] the band gap of BiOCl , $\text{Bi}_2\text{Ti}_2\text{O}_7$ and $\text{Bi}_2\text{Ti}_4\text{O}_{11}$ is 3.40, 2.90 and 3.24 eV, respectively. Then the equations^[33]: $E_{VB} = X - E_e + 0.5E_g$ and $E_{CB} = E_{VB} - E_g$ are applied to calculate the energy band edges of single semiconductor, where E_g is the band gap energy of semiconductor; E_{VB} is valence band (VB) edge potentials; E_{CB} is conduction band (CB) edge potentials; X is the electronegativity of semiconductor; E_e is the energy of free electrons on hydrogen scale (~ 4.5 eV). Thus, E_{CB}/E_{VB} of BiOCl , $\text{Bi}_2\text{Ti}_2\text{O}_7$ and $\text{Bi}_2\text{Ti}_4\text{O}_{11}$ are 0.18/3.58, -0.24/2.66 and -0.23/3.01 eV, respectively. The electrons cannot easily transfer from $\text{Bi}_2\text{Ti}_2\text{O}_7$ to $\text{Bi}_2\text{Ti}_4\text{O}_{11}$, due to their close CBM potentials. On the contrary, VBM and CBM potentials of BiOCl are both more positive than those of $\text{Bi}_2\text{Ti}_2\text{O}_7$. In that case, heterojunctions are formed at the interface between BiOCl and $\text{Bi}_2\text{Ti}_2\text{O}_7$, favoring charge transfer and significantly inhibiting electron-hole recombination rate.

The microstructural details of BT-500 are further characterized by TEM and HRTEM observation as shown in Fig.7. TEM image shows that BT-500 nanorods mainly consists of nanoparticles (Fig. 7a). As seen in Fig. 7b, the interplanar spacing of 0.267 and 0.344 nm corresponds to the (102) and (101) plane of BiOCl , while 0.298 and 0.236 nm corresponds to the respective (444) and (662) plane of $\text{Bi}_2\text{Ti}_2\text{O}_7$. The continuity of lattice fringes between the interface of BiOCl and $\text{Bi}_2\text{Ti}_2\text{O}_7$ can favor the charge transfers between them.

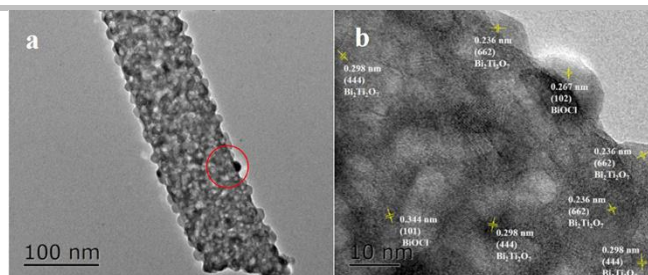


Figure 7. (a) TEM images and (b) HRTEM images of BT-500.

In order to better understand the photocatalytic mechanism of TC-HCl photodegradation over BT-500 under simulated solar irradiation, the trapping experiments of active species involved in the photocatalytic reaction are investigated.^[10, 34] In this study, Benzoquinone (BQ)^[35], ammonium oxalate (AO)^[36] and dimethyl sulfoxide (DMSO)^[37] acting as the scavengers for superoxide radicals ($\text{O}_2^{\cdot-}$), holes (h^+) and hydroxyl radicals ($\cdot\text{OH}$) are introduced into the photocatalytic process, respectively. From Fig.8, it is clearly that N_2 bubbling and excess BQ and AO show little effects on the degradation of TC-HCl compared with no scavenger at the same conditions, suggesting that $\text{O}_2^{\cdot-}$ and h^+ have a negligible effect on the TC-HCl photodegradation mechanism. On the contrary, the decomposition rate of TC-HCl decreases to 67% after the addition of DMSO. According to these results, it can be clearly seen that $\cdot\text{OH}$ radicals are main reactive species for BT-500 in the photodegradation process of TC-HCl.

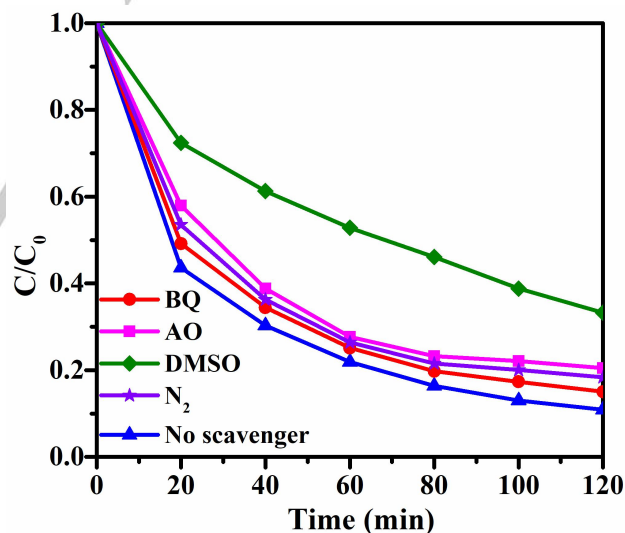


Figure 8. Effects of scavengers on the degradation of TC-HCl over BT-500.

The intermediates formed on BT-500 during the photocatalytic process is characterized by LC-HRMS. Fig. 9 shows the mass spectra of TC-HCl before and after 2 h photocatalytic treatment. The peak with m/z of 445 is regarded as the tetracycline hydrochloride molecule. After simulated solar light irradiation, the peak with m/z of 445 disappear, and a lot of extra peaks (such as $m/z = 481, 476, 437, 432, 393, 388, 349, 344, 327, 305, 283, 261, 217, 177, 133, 89$) appear along with the degradation of TC-HCl. The possible molecular structures of these products

FULL PAPER

WILEY-VCH

are described in Table S2. Combining with these detection results and references,^[38] the degradation removal process could be proposed as two main pathways (Fig. 10).

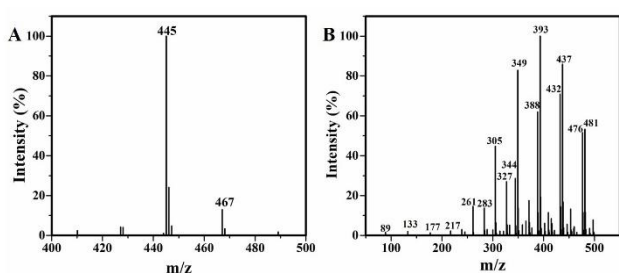


Figure 9. LC-HRMS spectra of TC-HCl, (A) before and (B) after photocatalysis.

The first pathway is primary degradation by addition of hydroxyl locating at C_{11a}-C₁₂ and C₂-C₃ double-bond of TC-HCl with attack of the •OH radicals to generate the intermediate with *m/z* 476, which is further fragmented to the product 2 (*m/z* 393) via deprivation of methyl from the tertiary amine and amide group. Subsequently, •OH attacks C₄ bond to cleave benzene rings and eliminate methyl, forming product 4 (*m/z* 344). Further degradation products (products 5-7, 14-16) with lower molecular weight result from the elimination of hydroxyl, N-methyl and cleavage of benzene rings. On the other hand, the product 2 (*m/z* 393) can also be decomposed to the detected product 3 with *m/z* 347 via cleavage of benzene rings, elimination of methyl, and the addition of hydroxyl and dehydration. The possible degradation pathways at this stage in terms of molecular weight (MW) can be expressed as follows: 445→476→393→347;

393→344→327→283→217→177→134→88.

The second pathway, •OH radicals attack the C_{11a}-C₁₂ double-bond of TC-HCl to add hydroxyl and remove methyl from the tertiary amine, generating the *m/z* 432 (product 8). Then, aromatic ring is attacked at C_{6a}-C₇ bond, in which gives rise to a ketone group and a carboxylic group at the C_{6a} and C₇ positions, respectively, yielding the product 9 with *m/z* 480. It is further decomposed to simpler intermediates (products 10-16) detected in the following reaction, such as the elimination of amide group, hydroxyl group, amidogen, ketone group, carboxylic group and methyl alcohol, and the substitution reaction by ring-opening reaction is also involved in this process. The possible degradation pathways at this stage are expressed as follows: 445→432→481→437→388→305→261→177→134→88.

Thus, it can be seen that TC-HCl has been gradually disintegrated, and the relevant degradation intermediates are produced and then decomposed. Finally, these substances can convert into CO₂, H₂O and the other degradation products.

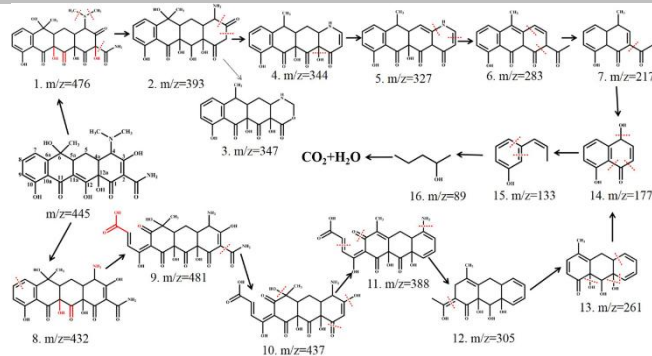


Figure 10. The removal pathway of TC-HCl over BT-500.

Based on the above results, a possible photocatalytic mechanism for BTs under simulated solar light is proposed in Fig.11. Under simulated solar light irradiation, BiOCl and Bi₂Ti₂O₇ can be excited by UV and visible light, respectively, generating the electrons and holes (Fig.11a). The electrons in the conduction band (CB) of Bi₂Ti₂O₇ shift to BiOCl due to the CBM of Bi₂Ti₂O₇ is more negative than that of BiOCl. Simultaneously, the holes in the VB of BiOCl move to Bi₂Ti₂O₇ due to the VBM of BiOCl is more positive than that of Bi₂Ti₂O₇. As a result, the photogenerated charge carriers are separated efficiently, and the electron-hole recombination rate is suppressed. However, since CB edges of Bi₂Ti₂O₇ and Bi₂Ti₄O₁₁ is very close, the photogenerated electrons transfer difficultly from Bi₂Ti₂O₇ to Bi₂Ti₄O₁₁, resulting in an unsatisfied charge separation (Fig.11b).

Although the photogenerated electrons are transferred to the CB of BiOCl, which cannot react with O₂ to produce O₂^{•-}, because the CBM potential of BiOCl (0.18 eV vs NHE) is more positive than E₀(O₂/O₂^{•-}) (-0.33 eV vs NHE).^[39] The photogenerated holes on the VB of BiOCl could be easily transferred to that of Bi₂Ti₂O₇, which can react with surface-adsorbed hydroxyl or H₂O to produce •OH.^[40] Then •OH directly involves in the degradation of TC-HCl. In this way, the efficient separation of photogenerated electron-hole pairs can be achieved, and the photocatalytic activity is improved.

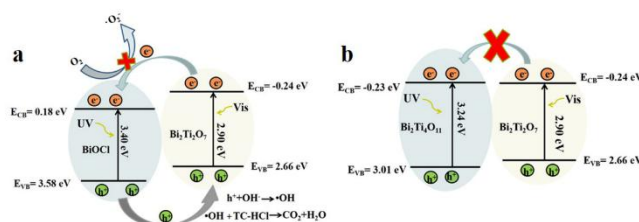


Figure 11. Photocatalytic mechanism scheme for the degradation of TC-HCl over (a) BiOCl/Bi₂Ti₂O₇, (b) Bi₂Ti₂O₇/Bi₂Ti₄O₁₁ under simulated solar light.

Besides excellent photocatalytic activity, photocatalysts also should display great photocatalytic stability. The stability is a very important factor for practical applications. In order to evaluate the stability of prepared catalysts, BT-500 is selected for the recycling test under simulated solar light, as shown in Fig.12A. The result shows that there is no obvious reduction of the photocatalytic degradation efficiency upon five recycling. Furthermore, the XRD patterns of the fresh and used BT-500

clearly indicates that the structure of BT-500 has no change (Fig. 12B). SEM image in Fig. 12C reveals that the morphology of used BT-500 is still featured by nanorods. These results indicate that the obtained BT-500 has good stability during the photocatalytic process.

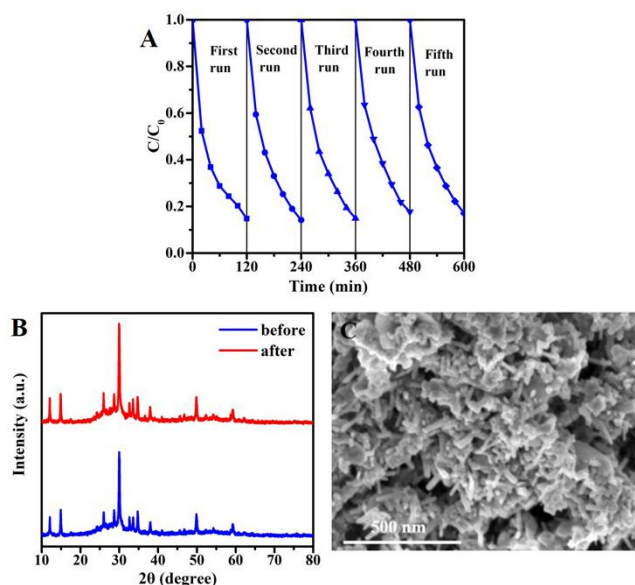


Figure 12. (A) Cycling runs in the photocatalytic degradation of TC-HCl under simulated solar light illumination of BT-500; (B) XRD patterns of BT-500: before photocatalysis and after cycling runs; (C) SEM image of used BT-500.

Conclusions

In this study, bismuth titanates with different phases can be tuned by an electrospinning combined with calcination route. After calcination at 400 °C, the smooth nanofibers of PVP/BiCl₃/Ti(OiPr)₄ break into BiOCl/Bi₂Ti₂O₇ nanorods. Further increasing calcination temperatures to 600-700 °C, the phase of Bi₂Ti₂O₇/Bi₂Ti₄O₁₁ is formed. The results of TC-HCl photodegradation under simulated solar irradiation indicate that BiOCl/Bi₂Ti₂O₇ shows higher photocatalytic performance than Bi₂Ti₂O₇/Bi₂Ti₄O₁₁. It is mainly thanks to the good match of energy levels between BiOCl and Bi₂Ti₂O₇ to form heterojunction structure, accelerating the separation of photogenerated electron-hole pairs. The enhanced charge separation efficiency was confirmed by PL spectra and photoelectrochemical measurements. The obtained BT-500 exhibits the excellent and good stable photocatalytic performance. Scavenger tests demonstrate that •OH plays the dominant role for the photodegradation of TC-HCl. The possible degradation pathway of TC-HCl over BT-500 was identified by LC-HRMS analysis. It mainly consists of losing of amide group, hydroxyl group, amidogen, carboxylic group, methyl etc. and cleavage of benzene rings with the attack of •OH radicals. This work provides new route for the construction of BiOCl/Bi₂Ti₂O₇ nanorod heterostructures and offers pathway of TC-HCl into photodegradation.

Experimental Section

Preparation

The bismuth titanates (BTs) were synthesized by an electrospinning method, followed by furnace treatment. In a typical process, 1mmol bismuth chloride (BiCl₃) was firstly dissolved in the solution containing 20 mL N, N dimethylformamide and 5 mL acetic acid. Then 2 g PVP (Mw: 1300000, Aldrich) was added to the above solution under stirring for 4 h to form homogenous solution, which is then mixed with 1 mmol tetrabutyl titanate (Ti(OiPr)₄) under continued stirring for another 2 h to form light yellow precursor solution. The precursor solution was electrospun under high voltage of 23 kV, and the distance between spinneret and collector was fixed at 15 cm with a flow rate of 1 mL h⁻¹. Finally, the collected electrospun composite fibers were calcined in air at different temperatures for 3 h with a heating rate of 2 °C min⁻¹. For simplicity, the samples obtained from different calcination temperatures (300-700 °C) were denoted as BT-300, BT-400, BT-500, BT-600 and BT-700, respectively.

Characterization

The phase of the samples was determined on an X-ray diffraction analyzer (XRD, D8 Advance, Bruker) using graphite monochromatized Cu K α radiation, the accelerating voltage and the applied current were 40 kV and 40 mA, respectively. The morphology of the samples was analyzed on a field emission scanning electron microscope (FESEM, JEOL, JSM-7500F). Transmission electron microscopy (TEM) and high-resolution transmission electron microscopy (HRTEM) images were obtained on a JEM-2100F transmission electron microscope with an accelerating voltage of 200 kV. X-ray photoelectron spectroscopy (XPS) was measured using a Thermo ESCALAB 250Xi XPS, and the C 1s peak at 284.8 eV of the adventitious carbon was referenced to rectify the binding energies. The UV-visible diffuse reflectance absorption features were investigated on a UV-visible spectrophotometer (Cary 500 Scan Spectrophotometers, Varian, USA). The specific surface areas were analyzed by N₂ gas adsorption-desorption at 77 K on a BELSORP-mini surface area analyzer (BELSORP Co., Japan). Photoluminescence (PL) spectra were recorded on RF-5301PC spectrophotometer using room temperature photoluminescence with a 280 nm excitation wavelength. The photoelectrochemical measurements of samples were investigated by a CHI600E electrochemical workstation with a conventional three-electrode process in a quartz cell. Samples were deposited on FTO photoanode used as a working electrode, while Pt foil and Ag/AgCl electrode served as counter electrode and reference electrode, respectively. A 0.1 M Na₂SO₄ aqueous solution was employed as the electrolyte. The working electrode was illuminated using a Beijing Perfectlight Co., PLS-SXE300C Xe lamp. The intermediates formed during the degradation of TC-HCl were monitored by Liquid chromatography-high resolution mass spectrometry (LC-HRMS, Agilent 6460 Triple Quad) with electrospray ionization (ESI) source and a EC-C18 column (3.0× 50 mm; 2.7 μ m). The mixture of methanol-water (30:70, v/v, 1% formic acid containing in water) was used as mobile phase with a flow rate of 1 mL min⁻¹.

Photocatalytic activity test

The photocatalytic activities of BTs were evaluated by the decomposition of 50 mg L⁻¹ TC-HCl solution. Simulated solar photocatalytic reactions were performed in a 100 mL Pyrex glass vessel containing 100 mL TC-HCl aqueous solution and 100 mg catalyst. Before the photocatalytic activity test, the suspension mixture was stirred in the dark for 1 h to reach the adsorption/desorption equilibrium. Then the suspension solution was irradiated by a 300 W Xe lamp (PLS-SXE300C, Perfectlight, China). During irradiation, a 4 mL suspension was withdrawn at 20 min intervals and centrifuged. The obtained supernatant was analyzed on a Shimadzu UV-1750 UV-vis spectrophotometer at a wavelength of 364 nm.

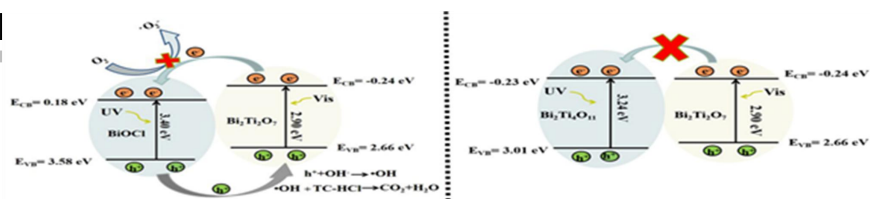
Acknowledgements

This work is supported by the National Science Foundation of China (21407025), the National Science Foundation of Fujian Province (2016J01047), and New Century Talent Project of Fujian Province.

Keywords: BiOCl/Bi₂Ti₂O₇ • heterostructure • solar photocatalysis • photocatalytic mechanism • removal pathway

- [1] a) E. M. H. Wellington, A. B. A. Boxall, P. Cross, E. J. Feil, W. H. Gaze, P. M. Hawkey, A. S. Johnson-Rollings, D. L. Jones, N. M. Lee, W. Otten, C. M. Thomas, A. P. Williams, *Lancet Infect. Dis.* **2013**, *13*, 155-165.; b) A. M. Hammerum, O. E. Heuer, *Clin. Infect. Dis.* **2009**, *48*, 916-921.; c) E. S. Elmolla, M. Chaudhuri, *Desalination* **2010**, *252*, 46-52.; d) P. Huo, Y. Yan, S. Li, H. Li, W. Huang, *Appl. Surf. Sci.* **2010**, *256*, 3380-3385.
- [2] Q. Zhang, G. Ying, C. Pan, Y. Liu, J. Zhao, *Environ. Sci. Technol.* **2015**, *49*, 6772-6782.
- [3] a) R. Daghrir, P. Drogui, *Environ. Chem. Lett.* **2013**, *11*, 209-227.; b) Q. Chen, X. Guo, G. Hua, G. Li, R. Feng, X. Liu, *Environ. Pollut.* **2017**, *220*, 1301-1310.
- [4] R. Gothwal, T. Shashidhar, *CLEAN – Soil, Air, Water* **2015**, *43*, 479-489.
- [5] A. Christou, A. Agüera, J. M. Bayona, E. Cytryn, V. Fotopoulos, D. Lambropoulou, C. M. Manaia, C. Michael, M. Revitt, P. Schröder, D. Fatta-Kassinos, *Water Res.* **2017**, *123*, 448-467.
- [6] Y. Wang, Q. Wang, X. Zhan, F. Wang, M. Safdar, J. He, *Nanoscale* **2013**, *5*, 8326-8339.
- [7] H. Huang, X. Han, X. Li, S. Wang, P. K. Chu, Y. Zhang, *ACS Appl. Mater. Interfaces* **2015**, *7*, 482-492.
- [8] a) H. Huang, K. Xiao, Y. He, T. Zhang, F. Dong, X. Du, Y. Zhang, *Appl. Catal. B: Environ.* **2016**, *199*, 75-86.; b) H. Huang, K. Xiao, T. Zhang, F. Dong, Y. Zhang, *Appl. Catal. B: Environ.* **2017**, *203*, 879-888. c) H. Huang, S. Tu, C. Zeng, T. Zhang, A. H. Reshak, Y. Zhang, *Angew. Chem. Int. Ed.* **2017**, *129*, 12022-12026.
- [9] L. Zhou, W. Wang, L. Zhang, *J. Mol. Catal. A: Chem* **2007**, *268*, 195-200.
- [10] H. Huang, X. Li, J. Wang, F. Dong, P. K. Chu, T. Zhang, Y. Zhang, *ACS Catal.* **2015**, *5*, 4094-4103.
- [11] Y. Fu, L. Peng, Q. Zeng, Y. Yang, H. Song, J. Shao, S. Liu, J. Gu, *Chem. Eng. J.* **2015**, *270*, 631-640.
- [12] S. Gupta, V. Subramanian, *ACS Appl. Mater. Interfaces* **2014**, *6*, 18597-18608.
- [13] F. Niu, D. Chen, L. Qin, N. Zhang, J. Wang, Z. Chen, Y. Huang, *ChemCatChem* **2015**, *7*, 3279-3289.
- [14] a) D. Zhou, H. Yang, Y. Tu, Y. Tian, Y. Cai, Z. Hu, X. Zhu, *Nanoscale res. Lett.* **2016**, *11*, 1-8.; b) Z. Zhang, C. Jiang, P. Du, Y. Wang, *Ceram. Int.* **2015**, *41*, 3932-3939.; c) H. Liu, Y. Chen, G. Tian, Z. Ren, C. Tian, H. Fu, *Langmuir* **2015**, *31*, 5962-5969.
- [15] a) H. Shi, H. Tan, W.-b. Zhu, Z. Sun, Y. Ma, E. Wang, *J. Mater. Chem. A* **2015**, *3*, 6586-6591.; b) Y. Liu, G. Zhu, J. Peng, J. Gao, C. Wang, P. Liu, *J Mater Sci: Mater Electron* **2017**, *28*, 2172-2182.
- [16] a) H. Peng, C. K. Chan, S. Meister, X. F. Zhang, Y. Cui, *Chem. Mater.* **2008**, *21*, 247-252.; b) Y. Yu, C. Cao, H. Liu, P. Li, F. Wei, Y. Jiang, W. Song, *J. Mater. Chem. A* **2014**, *2*, 1677-1681.
- [17] K. V. Pham, V. H. Nguyen, D. P. Nguyen, D. B. Do, M. O. Le, H. H. Luc, *J. Electron. Mater.* **2017**.
- [18] a) X. Zhang, V. Thavasi, S. G. Mhaisalkar, S. Ramakrishna, *Nanoscale* **2012**, *4*, 1707-1716.; b) J. Chen, H. B. Yang, J. Miao, H.-Y. Wang, B. Liu, *J. Am. Chem. Soc.* **2014**, *136*, 15310-15318.
- [19] L. Li, S. Peng, J. Wang, Y. L. Cheah, P. Teh, Y. Ko, C. Wong, M. Srinivasan, *ACS Appl. Mater. Interfaces* **2012**, *4*, 6005-6012.
- [20] a) Y. Xu, Z. Li, X. Liu, Y. Luo, Q. Qian, B. Huang, L. Xiao, Q. Chen, *J Mater Sci: Mater Electron* **2017**, *28*, 8596-8600.; b) X. Liu, Y. Chen, C. Cao, J. Xu, Q. Qian, Y. Luo, H. Xue, L. Xiao, Y. Chen, Q. Chen, *New J. Chem.* **2015**, *39*, 6944-6950.; c) Y. Luo, K. Wang, Y. Xu, X. Wang, Q. Qian, Q. Chen, *New J. Chem.* **2015**, *39*, 1001-1005.
- [21] U. G. Akpan, B. H. Hameed, *J. Hazard. Mater.* **2009**, *170*, 520-529.
- [22] a) Y. Qi, W. Wu, L. Han, H. Qu, X. Han, A. Wang, J. Xu, *J. Therm. Anal. Calorim.* **2016**, *123*, 1263-1271.; b) F. Gao, D. Zeng, Q. Huang, S. Tian, C. Xie, *Phys. Chem. Chem. Phys.* **2012**, *14*, 10572-10578.
- [23] L. Xu, Y. Wei, W. Guo, Y. Guo, Y. Guo, *Appl. Surf. Sci.* **2015**, *332*, 682-693.
- [24] S. K. Parayil, H. S. Kibombo, C.-M. Wu, R. Peng, J. Baltrusaitis, R. T. Koodali, *Int. J. Hydrogen Energy* **2012**, *37*, 8257-8267.
- [25] H. Zuo, J. Sun, K. Deng, R. Su, F. Wei, D. Wang, *Chem. Eng. Technol.* **2007**, *30*, 577-582.
- [26] P. Zhang, C. Shao, Z. Zhang, M. Zhang, J. Mu, Z. Guo, Y. Liu, *Nanoscale* **2011**, *3*, 2943-2949.
- [27] N. Liang, M. Wang, L. Jin, S. Huang, W. Chen, M. Xu, Q. He, J. Zai, N. Fang, X. Qian, *ACS Appl. Mater. Interfaces* **2014**, *6*, 11698-11705.
- [28] G.-w. Cui, W.-l. Wang, M.-y. Ma, M. Zhang, X.-y. Xia, F.-y. Han, X.-f. Shi, Y.-q. Zhao, Y.-B. Dong, B. Tang, *Chem. Commun.* **2013**, *49*, 6415-6417.
- [29] a) S.-F. Yang, C.-G. Niu, D.-W. Huang, H. Zhang, C. Liang, G.-M. Zeng, *Environ. Sci.: Nano* **2017**, *4*, 585-595.; b) T. C. Machado, T. M. Pizzolato, A. Arenzon, J. Segalin, M. A. Lansarin, *Sci. Total Environ.* **2015**, *502*, 571-577.
- [30] Y. Luo, Y. Xu, X. Liu, H. Xue, Q. Qian, Q. Chen, *J. Mater. Sci.* **2017**, *52*, 1265-1271.
- [31] D. Mao, A. Yu, S. Ding, F. Wang, S. Yang, C. Sun, H. He, Y. Liu, K. Yu, *Appl. Surf. Sci.* **2016**, *389*, 742-750.
- [32] a) C. Tan, G. Zhu, M. Hojamberdiev, K. Okada, J. Liang, X. Luo, P. Liu, Y. Liu, *Appl. Catal. B: Environ.* **2014**, *152*, 425-436.; b) T. Ghorai, D. Dhak, S. Dalai, P. Pramanik, *J. Alloys Compd.* **2008**, *463*, 390-397.
- [33] T. Yan, J. Tian, W. Guan, Z. Qiao, W. Li, J. You, B. Huang, *Appl. Catal. B: Environ.* **2017**, *202*, 84-94.
- [34] H. Huang, S. Tu, C. Zeng, T. Zhang, A. H. Reshak, Y. Zhang, *Angew. Chem. Int. Ed.* **2017**, *129*, 12022-12026.
- [35] a) X. Guo, Y. Chen, Z. Qin, J. Su, L. Guo, *ChemCatChem* **2016**, *8*, 3780-3789.
- [36] D. Sun, J. Li, L. He, B. Zhao, T. Wang, R. Li, S. Yin, Z. Feng, T. Sato, *CrystEngComm* **2014**, *16*, 7564-7574.
- [37] Y. Jiang, T.-P. Loh, *Chem. Sci.* **2014**, *5*, 4939-4943.
- [38] a) Y. Du, Q. Hao, D. Chen, T. Chen, S. Hao, J. Yang, H. Ding, W. Yao, J. Song, *Catal. Today* **2017**.; b) B. Gao, S. Dong, J. Liu, L. Liu, Q. Feng, N. Tan, T. Liu, L. Bo, L. Wang, *Chem. Eng. J.* **2016**, *304*, 826-840.; c) X. Wang, J. Jia, Y. Wang, *Chem. Eng. J.* **2017**, *315*, 274-282.; d) V. M. Mboula, V. Hequet, Y. Gru, R. Colin, Y. Andres, *J. Hazard. Mater.* **2012**, *209*, 355-364.
- [39] Z. Zhao, W. Zhang, Y. Sun, J. Yu, Y. Zhang, H. Wang, F. Dong, Z. Wu, *J. Phys. Chem. C* **2016**, *120*, 11889-11898.
- [40] H. Huang, Y. He, X. Li, M. Li, C. Zeng, F. Dong, X. Du, T. Zhang, Y. Zhang, *J. Mater. Chem. A* **2015**, *3*, 24547-24556.

Entry for the Table of Contents



Yuxian Xu, Daifeng Lin, Xinping Liu,
Yongjin Luo*, Hun Xue, Baoquan
Huang, Qinghua Chen, and Qingrong
Qian*

Page No. – Page No.

Title Electrospun BiOCl/Bi₂Ti₂O₇
nanorod heterostructures with
enhanced solar light efficiency in
photocatalytic degradation of
tetracycline hydrochloride